



$I_{Kr}$  is pharmacologically blocked (or set to zero in case of a model cell) and  $I_{HERG}$  is applied to the ventricular cell as an external current input. When wild-type (WT)  $I_{HERG}$  is added to the net membrane current of this ventricular cell, the resulting AP should be considered as normal, whereas a mutant  $I_{HERG}$  should cause distortion of the AP.

We applied our dAPC technique to the R56Q (arginine to glutamine) mutation, a defect known to increase the rate of deactivation most profoundly (Chen et al., 1999). Previously, R56Q HERG channels had only been expressed in *Xenopus* oocytes, and characterized at room temperature (Chen et al., 1999). We studied WT and mutant channels in HEK-293 cells also by conventional whole-cell voltage-clamp technique, at both 23 and 36°C. At physiological temperature, the mutant channels showed both faster deactivation, which would lengthen the AP, and faster activation, which by itself would shorten the AP. However, our dAPC experiments directly and unambiguously demonstrate that the net effect of the mutation is an increase in action potential duration (APD).

MATERIALS AND METHODS

Electrophysiological experiments

For details on plasmid construction, HEK-293 cell culture, and transfection procedures, see the expanded Materials and Methods, available as Supplementary Material online.

HEK-293 cells were either superfused with Tyrode's solution containing (mmol/L): 140 NaCl, 5.4 KCl, 1.8 CaCl<sub>2</sub>, 1 MgCl<sub>2</sub>, 5.5 glucose, 5 HEPES (pH 7.4 with NaOH), or with a modified Tyrode's solution with 4.5 instead of 5.4 mmol/L KCl (see below). Membrane currents were recorded with an Axopatch 200B amplifier (Axon Instruments, Union City, CA) in the whole-cell configuration of the patch-clamp technique at 23.5°C and 36.6°C. Voltage control, data acquisition, and analysis were accomplished using custom software. Patch pipettes (1.5 MΩ) were filled with solution containing (mmol/L): 125 K-gluconate, 20 KCl, 1 MgCl<sub>2</sub>, 5 EGTA, 5 MgATP, 10 HEPES (pH 7.2 with KOH), resulting in a K<sup>+</sup> equilibrium potential (E<sub>K</sub>) of -87.7 mV at 36°C. To obtain a better match between the E<sub>K</sub> of the experimental solutions and the model cell's maximum diastolic potential of -90.7 mV, we also used 4.5 mmol/L KCl in the Tyrode solution (resulting in an E<sub>K</sub> of -92.5 mV). All figures showing APs in the model-cell mode (see below) were obtained with this modified Tyrode solution. The p of solutions was corrected for temperature; potentials were corrected for liquid junction potential. Membrane currents and potentials were low-pass filtered (cutoff frequency 2 kHz) and digitized at 5 kHz. The current-voltage (I-V) relationships, and  $I_{HERG}$  kinetics were determined by voltage-clamp protocols, as diagrammed in Figs. 2 and 3, and as described previously (Sanguinetti et al., 1995; Smith et al., 1996; Snyders and Chaudhary, 1998) and in the Supplementary Material. APs from freshly isolated rabbit left ventricular myocytes were measured at 36°C with the solutions described above (5.4 mmol/L KCl in the Tyrode solution; EGTA was omitted in the pipette solution), as described previously (Verkerk et al., 1996) and detailed in the Supplementary Material.

Dynamic action potential clamp

Our approach is based on the coupling clamp (Tan and Joyner, 1990), model-cell mode (Wilders et al., 1996), and dynamic clamp (Sharp et al., 1993) techniques. The development of these techniques is built on the concept

of an isolated (cardiac) cell can be electrically coupled to either another isolated cardiac cell or to a model analog that mimics the electrical properties of the cardiac myocyte. As diagrammed in Fig. 1, a single cardiac ventricular cell and a transfected HEK-293 cell can be electrically coupled by means of an electrical circuit. The ventricular cell (with  $I_{Kr}$  blocked) is in current-clamp mode on one patch-clamp setup, whereas the HEK-293 cell is in voltage-clamp mode on another setup. The command potential for the HEK-293 cell is the  $V_m$  of the ventricular cell (action potential clamp), and the current input applied to the ventricular cell is the  $I_{HERG}$  recorded from the transfected HEK-293 cell, a connection resulting in dAPC condition (Fig. 1A). We performed two kinds of dAPC experiments, defined as real-cell mode and model-cell mode.

In model-cell mode (Fig. B), the ventricular cell is the Priebe-Beuckelmann (PB) model (Priebe and Beuckelmann, 1998) of a single human ventricular myocyte that is computed in real-time. We extended the model-clamp (Wilders et al., 1996) and dynamic clamp (Sharp et al., 1993) techniques,

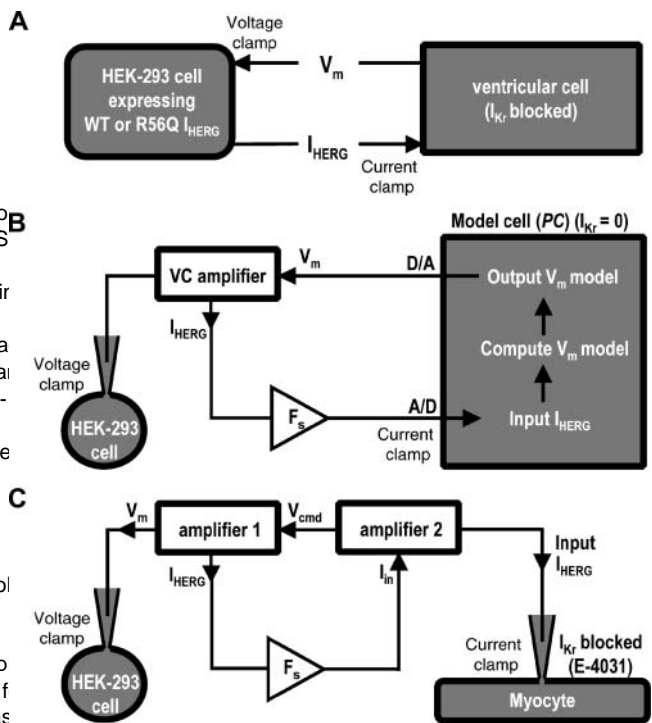
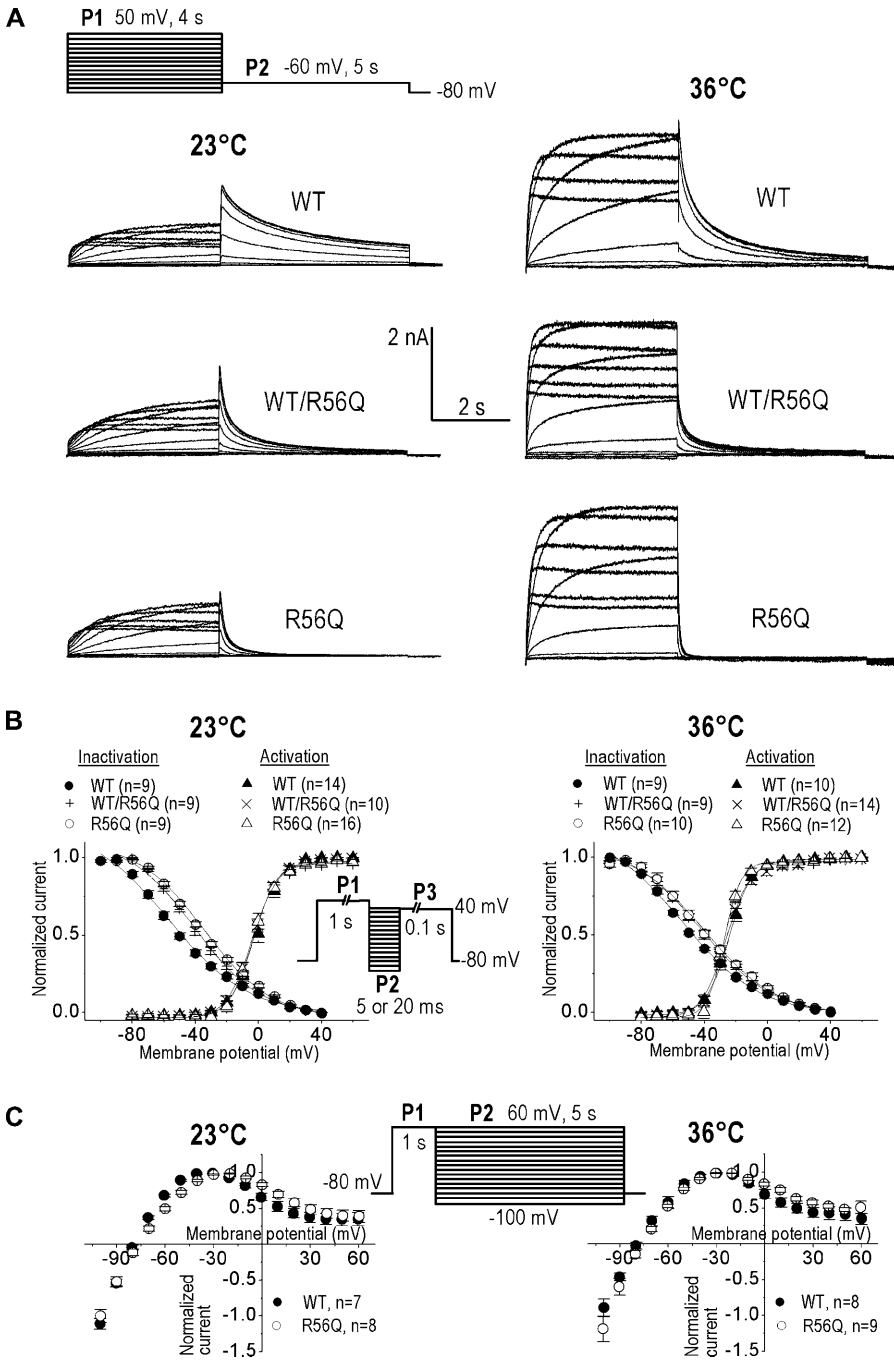


FIGURE 1 Diagram of the dAPC technique used to effectively replace the native  $I_{Kr}$  of a ventricular cell with  $I_{HERG}$  from a HEK-293 cell. A) Overall experimental design. B) Model-cell mode.  $I_{HERG}$  from a HEK-293 cell is recorded, scaled by a factor, and then digitized (A/D) by a computer (PC), which contains a model of the human ventricular cell (Priebe and Beuckelmann, 1998), with  $I_{Kr} = 0$ . The momentary  $V_m$  is computed in real-time using the model equations and the input  $I_{HERG}$ . The computed  $V_m$  is converted into an analog signal (D/A), sent back to the amplifier, and applied as a voltage-clamp command to the HEK-293 cell. C) Real-cell mode. The model cell has been replaced with a freshly isolated myocyte.  $I_{HERG}$  is recorded with amplifier 1, which is voltage-clamp mode, and scaled and applied as external current input (to amplifier 2, which is current-clamp mode). The  $V_m$  of the myocyte (with  $I_{Kr}$  blocked pharmacologically), shaped by the input  $I_{HERG}$  is applied as voltage-clamp command (to amplifier 1), thus establishing dAPC.



**FIGURE 2** Characteristics of WT and R56Q  $I_{HERG}$  at 23 and 36°C. (A) Representative examples of WT (top), WT/R56Q (middle), and R56Q (bottom) currents elicited by a two-step voltage-clamp protocol. P1-activated  $I_{HERG}$  steady-state current amplitude progressively increased and then decreased with depolarizing voltages, according to voltage-dependent inactivation. P2 elicited  $I_{HERG}$  tails; their peak is due to fast recovery from inactivation secondary to repolarization. The subsequent current decline is due to deactivation. (B) Voltage dependence of activation (protocol from inset) and inactivation (protocol from inset). See Table 1, for half-maximal (in)activation voltage and slope factor values. (C) I-V relationships (peak of  $I_{HERG}$  tails during P2 plotted against voltage) of R56Q and WT channels.

implementing dAPC with a real-time Linux operating system (Barabanov and Yodaiken, 1997) as a software platform according to Christini et al. (1999). To attain simultaneous control and recording of  $I_{HERG}$  and to resolve the time-critical tasks of analog-to-digital conversion of  $I_{HERG}$  calculation of the model, and digital-to-analog conversion of  $V_f$ , we developed a user program (DynaClamp). This was used with a real-time module that operates on a 1.8-GHz Pentium-4 PC with a 16-bit National Instruments PCI-6052E data acquisition board (National Instruments, Austin, TX) under real-time Linux, and communicated through shared memory and/or first-in, first-out scaling, the program establishes dAPC configuration between the model cell queues. This allows a guaranteed-timing real-time process (i.e., 40- $\mu$ s periodic time steps with the PB cell model). In all dAPC experiments of the model cell is set to zero. We first determine maximal  $I_{HERG}$  amplitude in the HEK-293 cell in voltage-clamp configuration, with 4-s depolarizing voltage steps to -10, 0, and 10 mV, from a holding potential of -80 mV, at 36.6  $\pm$  0.5  $^{\circ}$ C. Considering the unusual kinetics of HERG channels (Lu et al., 2001a), we measure  $I_{HERG}$  amplitudes at the end of 4-s pulses rather than from tail current amplitudes. The largest outward current value is then used to estimate the scaling factor  $k_f$  for the  $I_{HERG}$  input to the PB model cell. In our standard protocol, WT as well as R56Q  $I_{HERG}$  amplitude are scaled to 47.6 pA (equivalent to the original  $k_f$  amplitude in the PB model). After appropriate scaling, the program establishes dAPC configuration between the model cell queues. This allows a guaranteed-timing real-time process (i.e., 40- $\mu$ s periodic time steps with the PB cell model). In all dAPC experiments of the model cell is set to zero. We first determine maximal  $I_{HERG}$  amplitude in the HEK-293 cell for 10 s, during which a series of 2-ms, 4-nA, 1-Hz suprathreshold stimuli are applied to the computer model cell. The recorded  $I_{HERG}$  and computed PB model variables (and ionic currents) and settings

TABLE 1 Parameters of WT, R56Q, and WT/R56Q  $I_{HERG}$  activation and inactivation at 23 and 36 C

	23 C						36 C					
	WT		WT/R56Q		R56Q		WT		WT/R56Q		R56Q	
<b>Activation</b>												
$V_{1/2}$ (mV)	-1.16	1.1	-2.86	1.1	-3.96	1.0	-26.66	1.4	-28.16	1.0	-28.66	1.4
k (mV)	7.96	0.2	7.96	0.3	7.86	0.2	6.56	0.3	6.36	0.3	6.16	0.3
<b>Inactivation</b>												
$V_{1/2}$ (mV)	-56.66	2.1	-40.46	2.3	-34.56	1.7*	-49.66	2.6	-42.36	3.2	-39.86	3.2*
k (mV)	-24.56	1.5	-22.16	1.5	-22.56	1.5	-23.56	0.5	-22.86	0.7	-23.16	1.0

\*P, 0.05 for R56Q versus WT. Values are mean  $\pm$  SE; n, the number of experiments, see Fig. 2

of the DynaClamp program are stored on disk for off-line analysis. The time constants of the ventricular model cell are derived from WT APs in the myocyte at 1 Hz in the presence of E-4031, and then establish and/or mutant  $I_{HERG}$  input and the model equations. The combination of the coupling between the myocyte and the HEK-293 cell, implementing scaled cell model and WT  $I_{HERG}$  will then result in a normal AP. Using the same WT  $I_{HERG}$  A proper  $F_s$  value would result in  $I_{HERG}$  density comparable to method for HEK-293 cells with mutant channels will reveal an AP, which that of the  $I_{Kf}$  density in the myocyte and in a typical AP duration at 90% resembles the ventricular AP of the patient from which the mutant was derived.

Real-cell mode

In real-cell mode, the model cell is replaced with a rabbit left-ventricular myocyte (Fig. 1C). The procedure to determine  $I_{HERG}$  amplitude in the HEK-cell (as described above) and, simultaneously,  $V_m$  of the ventricular cell and  $I_{HERG}$  of HEK-293 cell are displayed on-

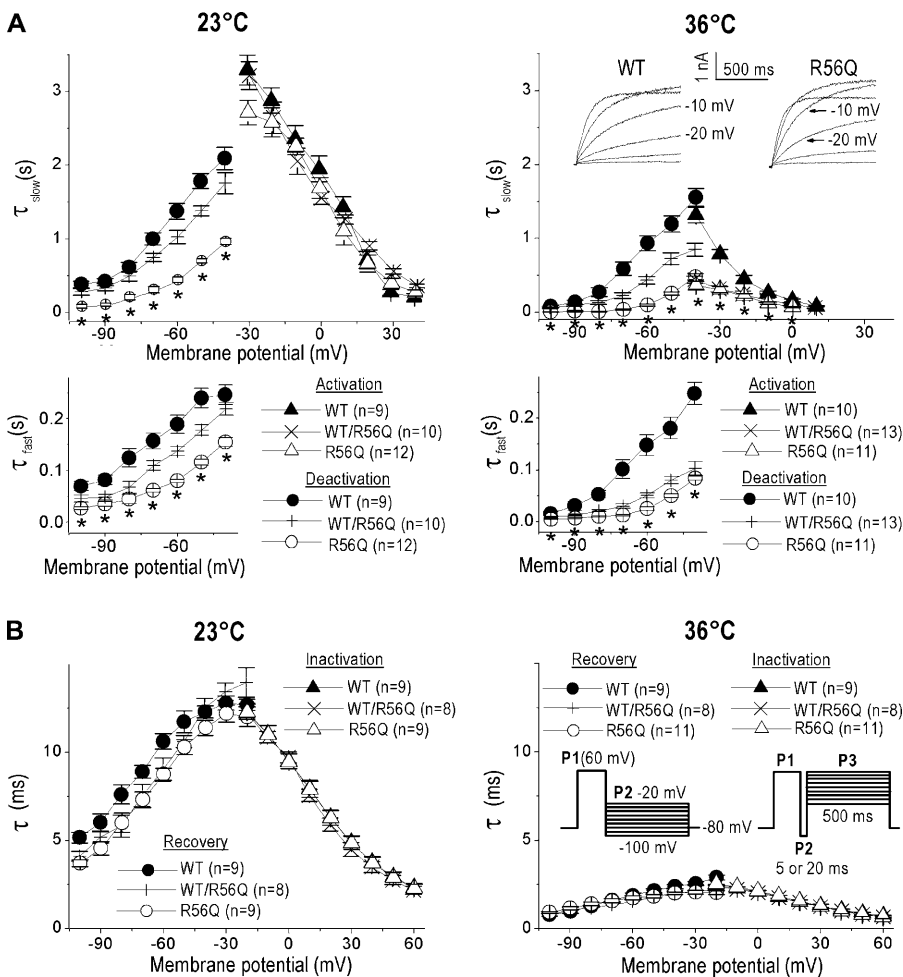


FIGURE 3 Time constants of WT and R56Q  $I_{HERG}$  kinetics at 23 and 36 C. (A) Time constant of activation ( $\tau_{slow}$ , triangles) and fast and slow time constant of deactivation ( $\tau_{fast}$  and  $\tau_{slow}$ , circles). Voltage-clamp protocols are shown in Fig. 2, A and C, respectively, and described in the Supplementary Material. Faster activation of R56Q HERG channels was apparent only at 36 (see current traces inset), whereas deactivation was faster for R56Q than for WT at both 23 and 36 (\*, significant difference for R56Q versus WT, P, 0.05). WT/R56Q showed a mixed phenotype. (B) Time constants of inactivation (triangles) and recovery from inactivation (circles). Voltage-clamp protocols are shown as insets and described in the Supplementary Material.

line, thus providing instant information on the dAPC. DynaClamp allows scaling of the input current to any desired magnitude and subtraction of artifacts (e.g., endogenous HEK-293 cell currents), before being applied to the ventricular cell. Leak subtraction, however, was not necessary as downscaling already reduced endogenous currents to negligible levels.

## Statistics

Data are expressed as mean  $\pm$  SE ( $n$ , number of cells) and considered significantly different if  $p < 0.05$  in ANOVA and Student's  $t$ -test.

## RESULTS

### Electrophysiological characterization of WT, R56Q, and WT/R56Q HERG channels

To investigate the influence of recording temperature and R56Q channels expression system on the WT and R56Q HERG channels (different).

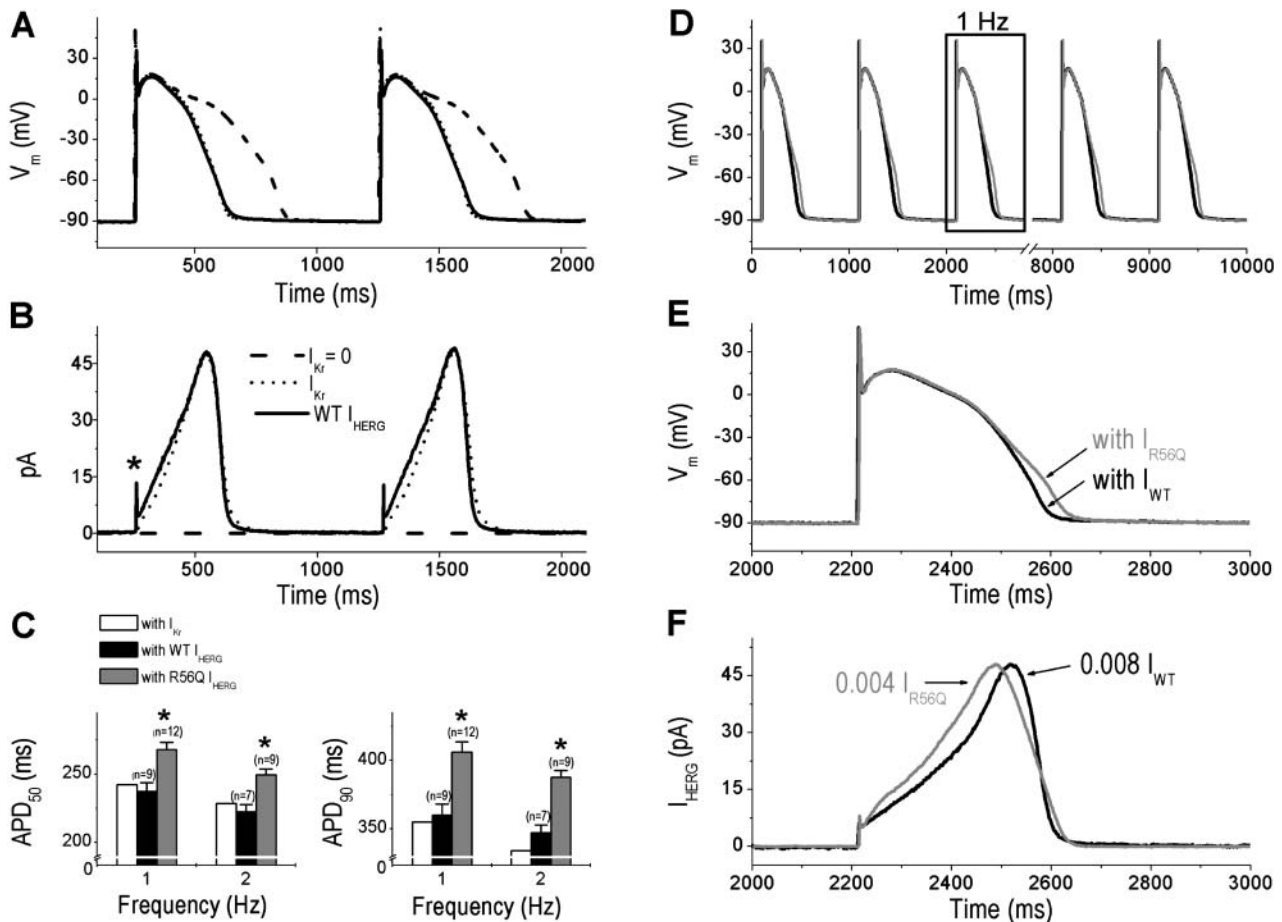


**FIGURE 4** The dAPC experiment with WT and R56Q HERG channels replacing  $I_{Kr}$  in the PB model cell. **A**) WT  $I_{HERG}$  is an effective substitute for  $I_{Kr}$ . Superimposed APs (at 1 Hz) in the absence of long dashed line) with  $I_{Kr}$  (short dashed line) or with WT  $I_{HERG}$  (solid line,  $I_{Kr} = 0$ ). **B**) Time course of the AP waveform-elicited WT  $I_{HERG}$  is similar to that of  $I_{Kr}$  in the PB cell model except for the early activation phase (asterisk). **C**) APD<sub>50</sub> and APD<sub>90</sub> values at 1 and 2 Hz (\*, significant difference for R56Q versus WT). **D**) Representative APs with WT  $I_{HERG}$  (solid line) or R56Q  $I_{HERG}$  (shaded line) at 1 Hz ( $I_{Kr} = 0$ ). **E** and **F**) Boxed APs from **D** (E) and associated  $I_{HERG}$  (F) on an expanded timescale. The HERG currents were scaled to identical maximal amplitude values (values indicated) and applied to the PB model cell as an external current input, and are thus responsible for repolarization of the model cell.

Time constants of  $I_{HERG}$  kinetics showed marked temperature dependence (Fig. 3). At 35°C the time course of R56Q channel activation was approximately threefold faster at all voltages than that of WT channels (Fig. 3 and see Table 1 in the Supplementary Material). For the heteromultimer WT/R56Q, the activation time constants were identical to those of R56Q alone. Remarkably, in *Xenopus* oocytes, the time course of R56Q channel activation was shown to be slower than for those of WT channels (Chen et al., 1999). The deactivation time course of R56Q channels was markedly faster than for those of WT at both temperatures, as shown by the diminution of both (fast and slow) time constants (Fig. 3 and see Table 1 in the Supplementary Material). The finding that the mutation causes faster deactivation is in agreement with the results of Chen et al. (1999). Time constants of inactivation and recovery from inactivation (Fig. 3) did not differ significantly between WT and R56Q (see Table 2 in the Supplementary Material). Our results demonstrate that acceleration of the R56Q HERG activation remains obscured at 23°C and highlight the importance of investigating HERG kinetics at physiological temperature.

Replacing  $I_{Kr}$  of the model cell with WT and R56Q  $I_{HERG}$

In the comprehensive human subepicardial ventricular cell model by Priebe and Beuckelmann (1998), description of which is based on data from human ventricular cells (Li et al., 1996). With model-cell  $I_{Kr}$  set to zero, the AP prolongs (Fig. 4 A). When WT  $I_{HERG}$  from a HEK-293 cell replaces  $I_{Kr}$ , AP characteristics are restored and the AP can be considered as normal (Fig. 4A and C). Similar results were obtained when the KCl content of the Tyrode solution was modified to 5.4 mmol/L (see, in Supplementary Material, Fig. 1 and Table 3). The time course of the scaled  $I_{HERG}$  compares well to that of  $I_{Kr}$  of the model cell (Fig. 4B) except that the initial time course of  $I_{HERG}$  differs from that of the mathematically described  $I_{Kr}$ , which is due to the model assumption that inactivation is instantaneous. Many HERG channels are still in the open state at 90 mV as a result of slow deactivation (Lu et al., 2001a), and this results in an initial transient peak (asterisk), reflecting the sudden increase of the electrochemical driving force for K during the AP upstroke. After a fast decay of the transient peak amplitude, caused by inactivation during the overshoot of the AP and by the decreasing driving force for K at less depolarized  $V_m$ , current increases progressively as channels rapidly recover from inactivation, a process faster than the deactivation (Sanguinetti et al., 1995; Trudeau et al., 1995; Smith et al., 1996; Zhou et al., 1998). With repolarization progressing, HERG channels dwell in a highly stable open state before closing (Wang et al., 1998), resulting in a resurgent current. Altered HERG channel properties in long-QT syndrome generally reduce the magnitude of this resurgent current.

TABLE 2 Relative densities of selected ionic currents in the subendocardial, M, and subepicardial cell models

Current	Subendocardial	Midmyocardial (M)	Subepicardial
$I_{to}$	25%; Nabauer et al. (1996)	87%; Liu et al. (1993)	100%
$I_{Ks}$	92%; Liu and Antzelevitch (1995)	46%; Liu and Antzelevitch (1995)	100%
$I_{K1}$	89%; Liu et al. (1993)	74%; Liu et al. (1993)	100%

All densities are percentage relative to the standard densities in the PB model that essentially describes a human subepicardial ventricular myocyte (Konrath et al., 2004).

(Chen et al., 1999; Sanguinetti et al., 1996). Both  $I_{HERG}$  reach maximum value  $-40$  mV, then rapidly deactivate in a time- and voltage-dependent manner.

To study the functional consequences of the R56Q mutation, we performed dAPC experiments with the PB cell model and WT and/or mutant  $I_{HERG}$  from the HEK-293 cell, in model-cell mode (Fig. 4D). Results of these experiments, remarkably consistent with the role of HERG channels in cardiac repolarization, clearly show that the AP is prolonged by the altered  $I_{HERG}$  kinetics of the mutant (Fig. 4C&E; see also Table 3 in the Supplementary Material). The WT or R56Q  $I_{HERG}$ , scaled to identical maximal amplitude values (Fig. 4F,  $F_s$  values indicated), was added to the PB model cell as an external current input, and thus contributed to repolarization of the model cell. Consistent with the results of voltage-clamp experiments at 35°C the input WT and R56Q  $I_{HERG}$  have different initial and late phases. Apparently, mutant  $I_{HERG}$  is initially larger than the WT. The faster

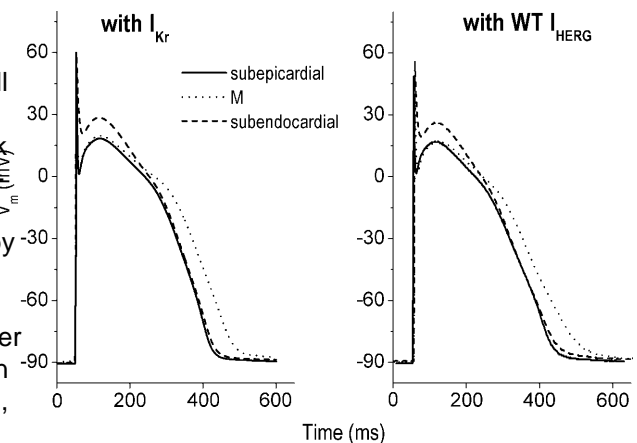


FIGURE 5 Regional AP heterogeneity is reproduced in a dAPC experiment. Subepicardial, M, and subendocardial APs were simulated at 1 Hz; note the different plateau levels and repolarization phases in these model cells (see the modified current densities in Table 2).

onset of the  $I_{HERG}$  decay indicates faster deactivation of the R56Q mutation on the AP characteristics of these cell types was AP prolongation (Fig. 6). We analyzed in detail AP characteristics of the epicardial model cell (Fig. 7), comparing the frequency dependence of  $APD_{90}$  values generated with model-cell<sub>Kr</sub> to values obtained with WT or R56Q  $I_{HERG}$ . These values are comparable when WT  $I_{HERG}$  is replaced by R56Q  $I_{HERG}$ , whereas R56Q  $I_{HERG}$  causes frequency-dependent  $APD_{90}$  prolongation (Fig. 7A).  $APD_{90}$  with the established. As in our previous model studies (Bernus et al., 2002; Conrath et al., 2004), we generated subendocardial values (not shown). The role of WT or R56Q  $I_{HERG}$  in midmyocardial (M), and subepicardial model cells by shaping the AP was evaluated by phase plane analysis adjusting selected membrane ionic currents in the PB model cell (Table 2). When, in a dAPC experiment, WT  $I_{HERG}$  currents against membrane potential (Fig. 7B) replaced model-cell<sub>Kr</sub>, APs of different shape and duration  $I_{HERG}$  scaled for identical amplitudes for both WT and R56Q, the consequence of the mutation is apparent. The

Action potential heterogeneity in the PB model cell with WT and R56Q  $I_{HERG}$

The heterogeneity of the electrical properties of the myocytes in the different layers of the human left ventricle is now well established. As in our previous model studies (Bernus et al., 2002; Conrath et al., 2004), we generated subendocardial (S), midmyocardial (M), and subepicardial model cells by shaping the AP was evaluated by phase plane analysis adjusting selected membrane ionic currents in the PB model cell (Table 2). When, in a dAPC experiment, WT  $I_{HERG}$  currents against membrane potential (Fig. 7B) replaced model-cell<sub>Kr</sub>, APs of different shape and duration  $I_{HERG}$  scaled for identical amplitudes for both WT and R56Q, the consequence of the mutation is apparent. The

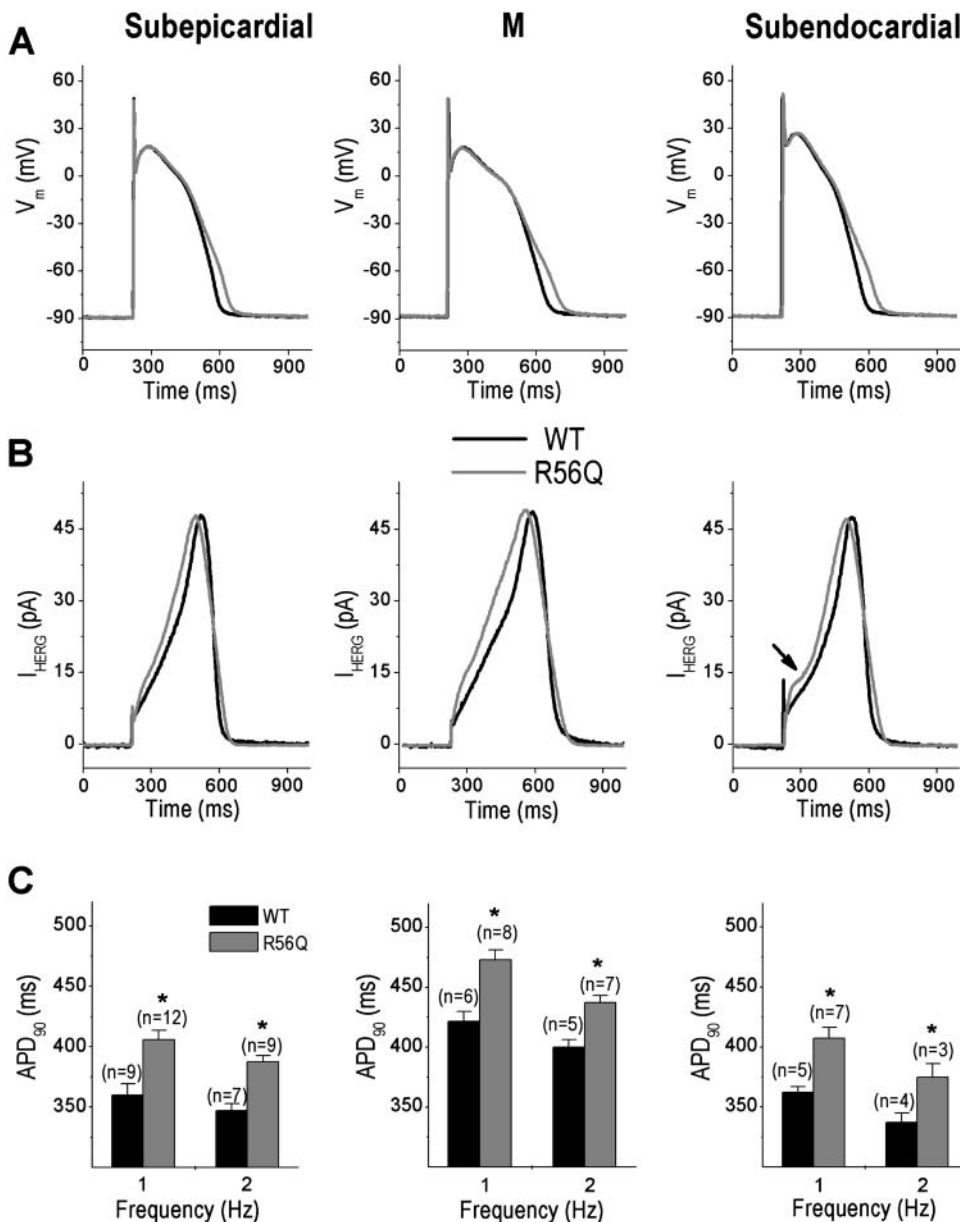


FIGURE 6 AP prolongation caused by the R56Q mutation in the three different cell types of Fig. 5. A) Representative APs and B) the corresponding  $I_{HERG}$ ; note the increased inactivation of R56Q  $I_{HERG}$  (arrow) at the positive plateau-voltages of the subendocardial cell; C) averaged  $APD_{90}$  values at 1 and 2 Hz (\*, significant difference for R56Q versus WT  $I_{HERG}$ ).

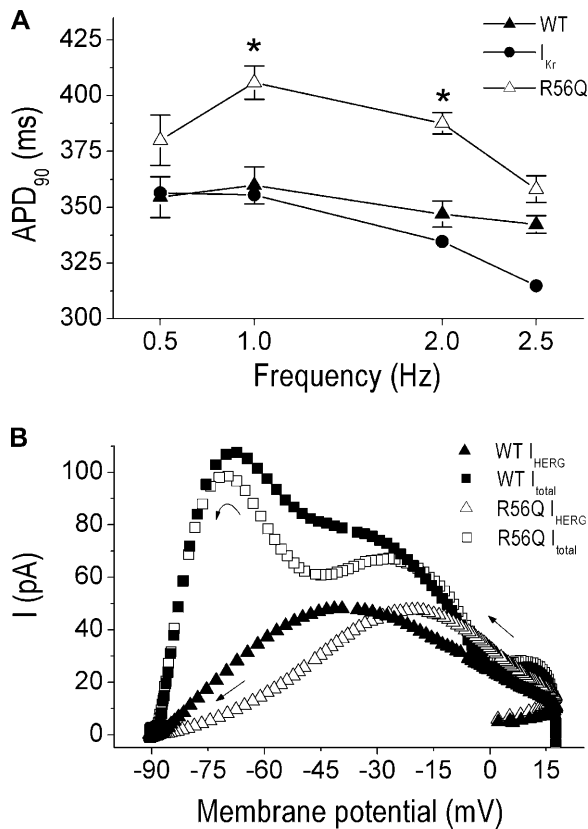


FIGURE 7 AP characteristics of the subepicardial PB model cell. (A) Frequency dependence with WT I<sub>HERG</sub> (n = 10), or R56Q I<sub>HERG</sub> (n = 8) (\*, significant difference for R56Q versus WT). (B) Phase-plane plot for the net membrane current (I<sub>total</sub>) and I<sub>HERG</sub> during repolarization (starting from +18 mV during phase-1 repolarization). APs from which these phase planes were obtained were generated at 1 Hz and are shown in Fig. 8, E. Arrows indicate progression of time.

most notable changes are detected during phase-3 repolarization, with a reduction of the net membrane current (I<sub>total</sub>).

Replacing I<sub>Kr</sub> of a rabbit ventricular cell with WT and R56Q I<sub>HERG</sub>

Results with I<sub>HERG</sub> replacing I<sub>Kr</sub> in the model cell show that the overall properties of the AP are well reproduced in a dAPC experiment (Figs. 4 and 5). Next, we used the real-cell variant of the technique (Fig. 8). Ionic currents underlying APs of a rabbit ventricular cell are comparable with those in a human ventricular cell. Fig. 8 shows typical whole-cell currents during 4-s depolarizing prepulses to 0 mV and tail currents after returning to -60 mV. I<sub>Kr</sub> may be differentially expressed in rabbit ventricles (Cheng et al., 1999), thus we first demonstrate its presence as the E-4031 sensitive current (Clay et al., 1995). Currents during depolarization as well as tails were markedly diminished in the presence of E-4031, resulting in prolonged repolarization and early after-depolarizations in all cells tested (Fig. 9).

(Fig. 8 B). dAPC experiments (n = 5) were performed with a single myocyte coupled first to a HEK-293 cell with WT I<sub>HERG</sub> (Fig. 8 C), and then to a HEK-293 cell with R56Q I<sub>HERG</sub> (Fig. 8 D). In both cases, AP parameters were determined at different stimulation frequencies (Fig. 9; see also Table 4 in the Supplementary Material). The measured resting V<sub>m</sub> of the myocytes was 82.96 ± 2.7 mV. APs were effectively reconstituted in a dAPC experiment with WT I<sub>HERG</sub>. APs with R56Q I<sub>HERG</sub> exhibited significant APD prolongation at 0.2 and 1 Hz (Fig. 9). These experiments also revealed that WT I<sub>HERG</sub> consists of an early fast transient outward current followed by a sustained outward current (Figs. 8 C and 9). Transient I<sub>HERG</sub> may contribute importantly to AP dynamics during tachycardia (Lu et al., 2001a). Amplitude of the transient component showed positive frequency dependence (Fig. 9) whereas that of the sustained component peaked during the terminal AP repolarization, in a reverse frequency-dependent manner between 1 and 5 Hz (Fig. 9). Although frequency dependence of the sustained R56Q I<sub>HERG</sub> was similar to that of WT I<sub>HERG</sub>, frequency dependence of the R56Q I<sub>HERG</sub> transient component was absent, consistent with the impaired deactivation kinetics of these channels.

DISCUSSION

A broad agreement prevails on the role of HERG channels in AP repolarization. For a better understanding of the link between LQT2 mutations and the inherent clinical phenotype, insight into the nature of HERG channel (dys)function is indispensable. As a longstanding approach, the time- and voltage-dependence of the HERG channel has most frequently been characterized using stepwise voltage-clamp protocols, and description of the HERG current was often based on the extrapolation of results obtained in various heterologous expression systems. However, it is becoming clear that complex features of HERG channel kinetics during the cardiac AP can best be studied during physiological voltage waveforms (Hancox et al., 1998; Lu et al., 2001a; Zhou et al., 1998) and, as shown in the present study, even better during dAPC condition (i.e., by letting them shape the ventricular action potential), in line with their normal function. The NH<sub>2</sub> terminus of the α-subunit of the channel regulates deactivation gating and represents a mechanism by which functional diversity is generated in HERG and related channels (Wang et al., 1998). Our electrophysiological experiments demonstrate that the R56Q mutation impairs not only deactivation (Chen et al., 1999) but also activation kinetics as well, the latter becoming apparent in the positive shift in the voltage dependence of channel inactivation (Fig. 2B), would actually act to shorten AP duration. Characteristics of the heteromultimeric (WT/R56Q) channels suggest that some of the functional effects

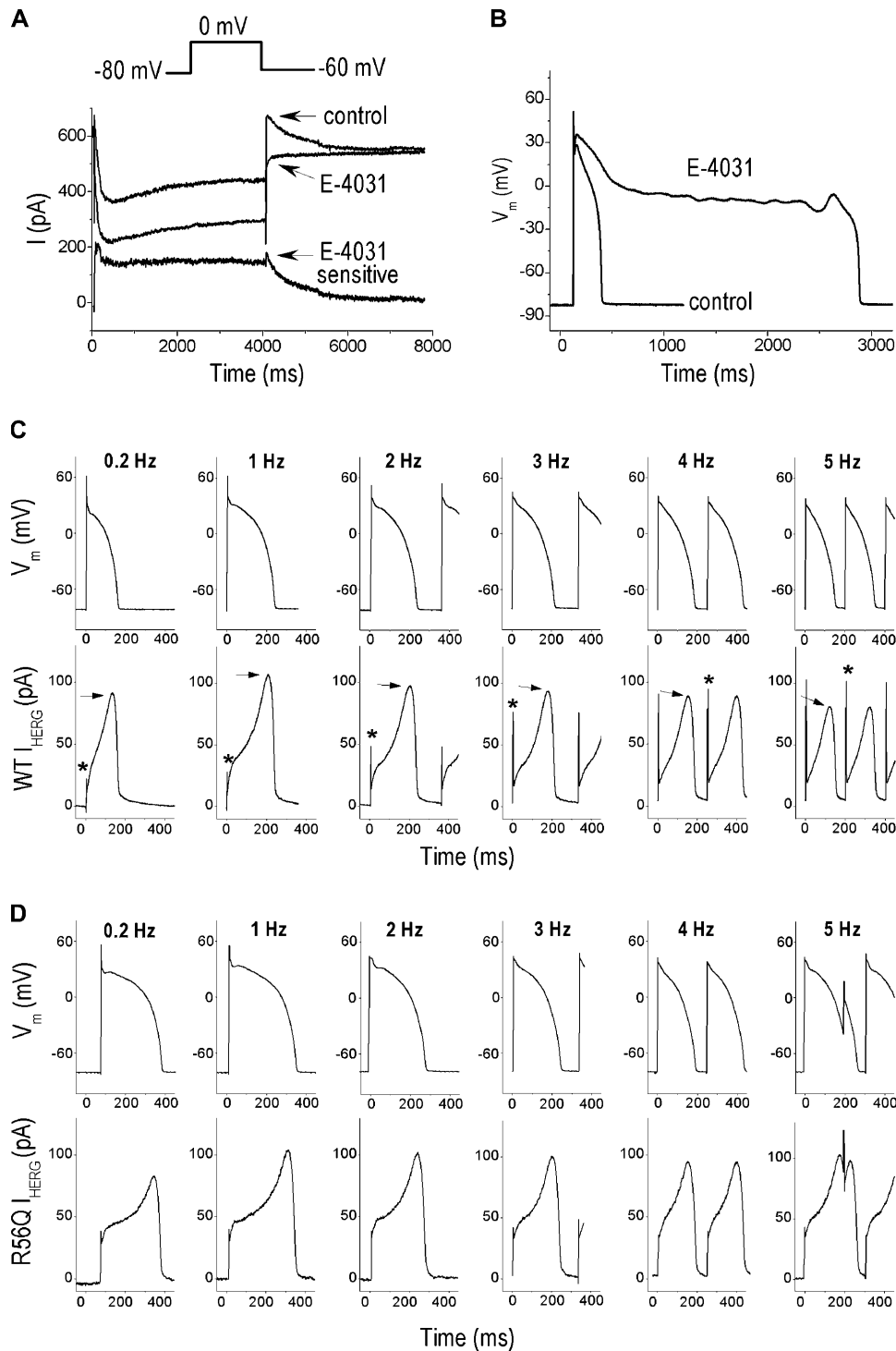


**FIGURE 8** The dAPC experiment with  $I_{HERG}$  replacing  $I_{Kr}$  in rabbit myocytes. **A)** Block of  $I_{Kr}$  with 5 mmol/L E-4031 (inset pulse protocol). Superimposed tracings of typical recordings in absence (control) and presence of E-4031, and difference (E-4031 sensitive) current. Mean  $I_{Kr}$  density, determined from the E-4031 sensitive current, was  $0.63 \pm 0.1$  pA/pF ( $n = 9$ ). **(B)** APs in a myocyte stimulated at 0.2 Hz before and after applying E-4031. Superfusion of cells with E-4031 caused early after-depolarizations. **(C and D)** APs from a myocyte and associated WT or R56Q  $I_{HERG}$  (**D**) at different frequencies. The myocyte was successively coupled to HEK-293 cells transfected with WT or R56Q HERG channels. Note the different  $I_{HERG}$  waveforms (\*, transient  $I_{HERG}$ ; arrow, sustained  $I_{HERG}$ ) and frequency-dependent AP prolongation with R56Q (see also Table 2 in the Supplementary Material).

are not simply combined, but that a dominant negative difference in  $I_{HERG}$  densities of WT and/or R56Q channels, interaction can also occur between the WT and R56Q HERG channels (see activation time constants at 36 Fig. 3A). suggesting that the primary defect in mutant channel properties is attributable to altered gating. Along the same lines with the impaired biophysical MinK-related peptide (MiRP1)/HERG complexes have properties, certain mutations in the Per-Arnt-Sim domain received considerable support as molecular correlates for might actually cause an HERG protein trafficking defect in  $I_{Kr}$  (Abbott et al., 1999, 2001). We did not coexpress (Paulussen et al., 2002). However, we did not find significant MiRP1 for reconstitution of native  $I_{Kr}$  by HERG, as

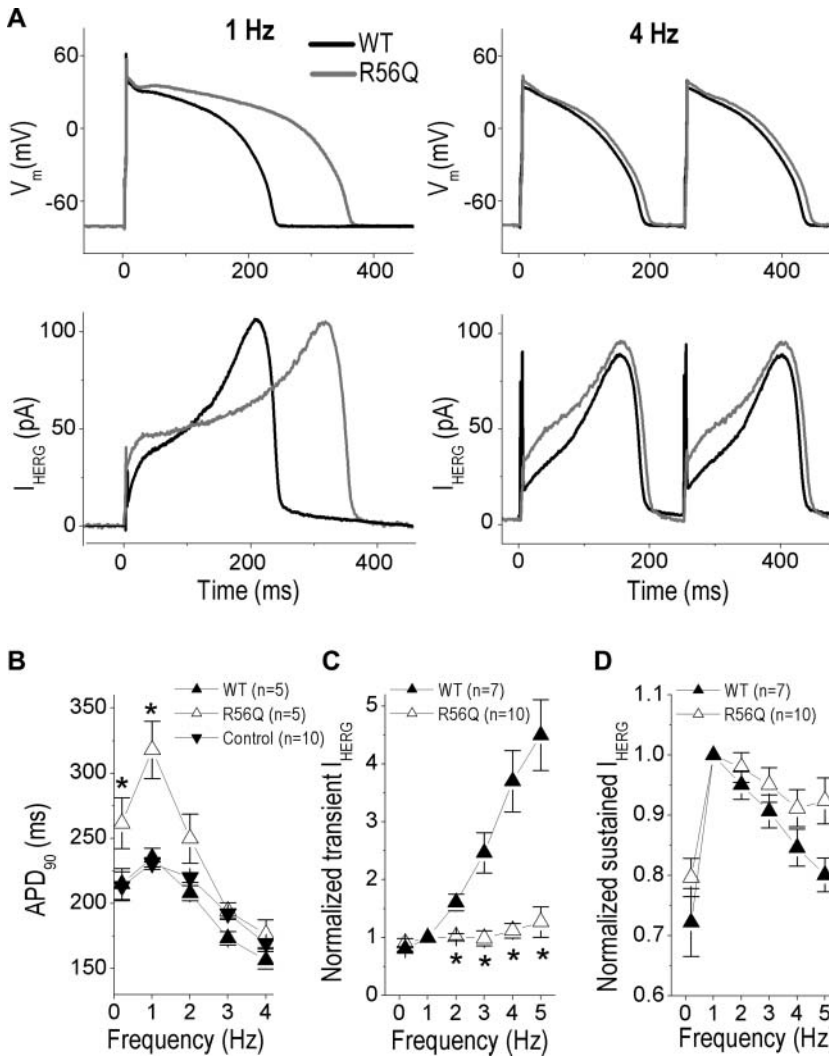


FIGURE 9 Action potential characteristics of rabbit ventricular myocytes with WT and R56Q<sub>HERG</sub>. (A) Superimposed APs from a single myocyte successively coupled to HEK-293 cells expressing WT (solid line) or R56Q<sub>HERG</sub> (shaded line) and the corresponding I<sub>HERG</sub> waveforms at 1 and 4 Hz. (B) Frequency dependence of APD<sub>90</sub> prolongation (□) and transient (▲) and sustained (○) I<sub>HERG</sub> amplitudes, each normalized to their values at 1 Hz. Asterisks indicate significant difference for R56Q versus WT.

properties of I<sub>HERG</sub> in mammalian systems are similar in many ways to those of native I<sub>Kr</sub>, and discrepancies that remain cannot be fully abolished by coexpression with alternative mammalian cell line, although 36°C for oocytes is not physiological, (Zhou et al., 1998; this study). Necessarily, the Xenopus system can be an alternative when channels do not express well in a mammalian cell line, although 36°C for oocytes is not physiological, (Zhou et al., 1998; this study).

Most experimental data on cardiac ion channel (dys)function have been obtained in expression systems, away from the cardiac environment where these channels function. The cellular environment where these channels function in oocytes dictate channel properties to some extent generate the cardiac action potential. Table 3 shows a comparison of I<sub>Kr</sub> in the various systems: 1), PB model; 2), human ventricle; 3), rabbit ventricle; and 4), HEK-293 cells. The relatively few studies of human ventricular cells make it difficult to fully validate such comparison. Nevertheless, the study of lost et al. (1998) provides data on human ventricular tissue obtained from healthy patients not receiving medication. Despite the apparent differences between some properties of I<sub>HERG</sub> and I<sub>Kr</sub> in the present study and previous results in the literature, mammalian cell lines generally provide an adequate environment for HERG channels. Here, experiments should be performed at physiological temperatures, as HERG channel gating is severely affected by the mutation during the late repolarization phase. APD values with R56Q<sub>HERG</sub> were

TABLE 3 Biophysical properties of  $I_{Kr}$  (in the PB ventricular model cell or in freshly isolated myocytes) and  $I_{HERG}$  (transiently expressed in HEK-293 cells)

	$I_{density}$ (pA/pF)	Activation	Inactivation	Deactivation	References
Model $I_{Kr}$	0.31				Priebe and Beuckelmann (1998); This study
$V_{1/2}$ (mV)		-21.0	-26.0		
k (mV)		5.4	-23.0		
t (ms)		194.5 (1 50 mV)		494.2 (-40 mV)	
Human $I_{Kr}$	; 0.3				Li et al. (1996); lost et al. (1998)
$V_{1/2}$ (mV)		-14.06 4, -5.7 <sup>y</sup>	ND		
k (mV)		7.76 2.7, 5.6*	ND		
t (ms)		192.06 53 (1 50 mV)		600.06 54 (-40 mV)*	
Rabbit $I_{Kr}$	0.3, 0.6				Lu et al. (2001b); This study
$V_{1/2}$ (mV)		-21.9	ND		
k (mV)		ND	ND		
t <sub>1</sub> (ms)		78.06 4 (1 50 mV)		119.06 25 (-50 mV)	
t <sub>2</sub> (ms)		624.06 42 (1 50 mV)		569.06 123 (-50 mV)	
WT $I_{HERG}$	2696 42				Zhou et al. (1998); This study
$V_{1/2}$ (mV)		-25.96 2.0 <sup>z</sup> , -26.66 1.4	-49.66 2.6		
k (mV)		6.06 0.3 <sup>z</sup> , 6.56 0.3	-23.56 0.5		
t <sub>1</sub> (ms)		18.06 3.0 (1 40 mV) <sup>z</sup>		180.06 20 <sup>z</sup> (-40 mV)	
t <sub>2</sub> (ms)				12996 118 <sup>z</sup> (-40 mV)	

Values are mean  $\pm$  SE; ND, not determined. All experiments were done under comparable conditions: 340 mM intracellular K concentration, 4 mM extracellular divalent cation concentration, 2 mM D3 mmol/L. Current density ( $I_{density}$ ) was defined as current level at the end of a 200 ms depolarizing pulse normalized to cell capacitance.

\*lost et al. (1998).

<sup>y</sup>Note that lost et al. (1998) did not mention any correction for liquid junction potential (LJP). (Taking into account an LJP of -10 mV under the given ionic conditions (Barry and Lynch, 1991), the actual  $V_{1/2}$  would be -16 mV.

<sup>z</sup>This study.

<sup>z</sup>Zhou et al. (1998)

increased at lower stimulation rates and unchanged at higher frequencies. Consistent with the role of HERG in the protocols become apparent with the dAPC technique. The suppression of arrhythmias initiated by premature beats (Lu et al., 2001a), the technique revealed the presence of an early afterdepolarization (EAD) during experimentation, as the input WT or mutant fast, frequency-dependent transient  $I_{HERG}$ . The frequency-dependent increase of this current component was absent with R56Q channels. APs with R56Q were generally longer (Fig. 8), which can be explained by the faster deactivation. However, the reason why the faster activation, thus initially larger  $I_{HERG}$  does not have a significant effect on the AP plateau is less obvious. It is likely that the faster activation of the R56Q  $I_{HERG}$  in the myocyte causes a slightly modified membrane potential in the early plateau phase of the AP, influencing activation of other currents.

Computer simulations using either the PB model or the recently published human ventricular cell model by Tusscher et al. (2004) also predict little or no effect of a moderate increase  $I_{Kr}$  during the plateau phase of the HERG, e.g., increasing the slow repolarizing component in a moderate increase  $I_{Kr}$  during the plateau phase of the HERG, e.g., increasing the slow repolarizing component (data not shown). On the other hand, even small changes of the myocyte membrane potential can cause significant changes in activation of voltage-dependent currents, such as the transient outward current (Flepp et al., 2000) and calcium current (Flepp et al., 2003).

In summary, both the computed model of the human ventricular cell as well as a freshly isolated myocyte can effectively be used in dAPC experiments. Kinetic features and the altered shape of AP directly reflects the effect of the

mutation. The dAPC technique allows other cardiac ion channels than HERG (e.g., SCN5A, KvLQT1) to be studied as well.

### General considerations

The inherent limitations of the PB model and of simulations when creating transmural AP heterogeneity on the basis of experimental findings have been discussed before (Bernus et al., 2002; Priebe and Beuckelmann, 1998). During dAPC experiments, in both model-cell and real-cell modes, we assumed that the defect in the R56Q channel is attributed to altered gating. Accordingly, we scaled WT and mutant input  $I_{HERG}$  to similar magnitudes.

We are aware that it is potentially conceivable that a mutation in an ion channel gene could result in compensatory changes in other ion channel genes in vivo, representing a general limitation of any heterologous expression system. Short-term alteration of mRNA levels of ion channels, caused by rapid pacing, is well documented (Yamashita et al., 2000). Libbus et al. (2004) provide direct evidence for remodeling in the ventricle caused by reduced AP upstroke amplitude, on a surprisingly short timescale.

### SUPPLEMENTARY MATERIAL

An online supplement to this article can be found by visiting BJ Online at <http://www.biophysj.org>.

This work was supported by Netherlands Heart Foundation grant No. 2001B155.

### REFERENCES

- Abbott, G. W., S. A. Goldstein, and F. Sesti. 2001. Do all voltage-gated potassium channels use MiRP1? *Circ. Res.*88:981D993.
- Abbott, G. W., F. Sesti, I. Splawski, M. E. Buck, M. H. Lehmann, K. W. Timothy, M. T. Keating, and S. A. Goldstein. 1999. MiRP1 forms a potassium channel with HERG and is associated with cardiac arrhythmia. *Cell.* 97:175D187.
- Barabanov, M., and V. Yodaiken. 1997. Introducing real-time Linux. *J.* 34:19D23.
- Barry, P. H., and J. W. Lynch. 1991. Liquid junction potentials and small cell effects in patch-clamp analysis. *Membr. Biol.*121:101D117.
- Bernus, O., R. Wilders, C. W. Zemlin, H. Verschelde, and A. V. Panfilov. 2002. A computationally efficient electrophysiological model of human ventricular cells. *Am. J. Physiol. Heart Circ. Physiol.*282:H2296D H2308.
- Chen, J., A. Zou, I. Splawski, M. T. Keating, and M. C. Sanguinetti. 1999. Long QT syndrome-associated mutations in the Per-Amt-Sim (PAS) domain of HERG potassium channels accelerate channel deactivation. *J. Biol. Chem.*274:10113D10118.
- Cheng, J., K. Kamiya, W. Liu, Y. Tsuji, J. Toyama, and I. Kodama. 1999. Heterogeneous distribution of the two components of delayed rectifier  $K^+$  current: a potential mechanism of the proarrhythmic effects of methanesulfonanilide Class III antiarrhythmics. *Cardiovasc. Res.*43:135D147.
- Christini, D. J., K. M. Stein, S. M. Markowitz, and B. B. Lerman. 1999. Practical real-time computing system for biomedical experiment interface. *Ann. Biomed. Eng.*27:180D186.
- Clancy, C. E., and Y. Rudy. 2001. Cellular consequences of HERG mutations in the long QT syndrome: precursors to sudden cardiac death. *Cardiovasc. Res.*50:301D313.
- Clay, J. R., A. Ogbaghebril, T. Paquette, B. I. Sasyniuk, and A. Shrier. 1995. A quantitative description of the E-4031-sensitive repolarization current in rabbit ventricular myocytes. *Biophys. J.*69:1830D1837.
- Conrath, C. E., R. Wilders, R. Coronel, J. M. De Bakker, P. Taggart, J. R. De Groot, and T. Opthof. 2004. Intercellular coupling through gap junctions masks M cells in the human heart. *Cardiovasc. Res.*62:407D 414.
- Curran, M. E., I. Splawski, K. W. Timothy, G. M. Vincent, E. D. Green, and M. T. Keating. 1995. A molecular basis for cardiac arrhythmia: HERG mutations cause long QT syndrome. *Cell.* 80:795D803.
- Felop, L., T. Benes, J. Magyar, N. Szentandassy, A. Varro and P. P. Nemesi. 2003. Reopening of L-type calcium channels in human ventricular myocytes during applied epicardial action potential. *Acta Physiol. Scand.*179:1D9.
- Greenstein, J. L., R. Wu, S. Po, G. F. Tomaselli, and R. L. Winslow. 2000. Role of the calcium-independent transient outward current in shaping action potential morphology and duration. *Circ. Res.*87:1026D1033.
- Hancox, J. C., A. J. Levi, and H. J. Witchel. 1998. Time course and voltage dependence of expressed HERG current compared with native  $I_{Kr}$  and  $I_{Ks}$  current during the cardiac ventricular action potential. *Pflügers Arch.*436:843D853.
- Host, N., L. Virag, M. Opincariu, J. Szosi, A. Varro and J. G. Papp. 1998. Delayed rectifier potassium current in undiseased human ventricular myocytes. *Cardiovasc. Res.*40:508D515.
- Li, G. R., J. Feng, L. Yue, M. Carrier, and S. Nattel. 1996. Evidence for two components of delayed rectifier  $K^+$  current in human ventricular myocytes. *Circ. Res.*78:689D696.
- Libbus, I., X. Wan, and D. S. Rosenbaum. 2004. Electrotonic load triggers remodeling of repolarizing current in ventricle. *Am. J. Physiol. Heart Circ. Physiol.*286:H1901D H1909.
- Liu, D. W., and C. Antzelevitch. 1995. Characteristics of the delayed rectifier current ( $I_{Kr}$  and  $I_{Ks}$ ) in canine ventricular epicardial, mid-myocardial, and endocardial myocytes. A weak  $I_{Kr}$  contributes to the longer action potential of the cell. *Circ. Res.*76:351D365.
- Liu, D. W., G. A. Gintant, and C. Antzelevitch. 1993. Ionic bases for electrophysiological distinctions among epicardial, midmyocardial, and endocardial myocytes from the free wall of the canine left ventricle. *Circ. Res.*72:671D687.
- Lu, Y., M. P. Mahaut-Smith, A. Varghese, C. L. Huang, P. R. Kemp, and J. I. Vandenberg. 2001a. Effects of premature stimulation on HERG K channels. *J. Physiol.*537:843D851.
- Lu, Z., K. Kamiya, T. Opthof, K. Yasui, and I. Kodama. 2001b. Density and kinetics of  $I_{Kr}$  and  $I_{Ks}$  in guinea pig and rabbit ventricular myocytes explain different efficacy of  $K^+$  blockade at high heart rate in guinea pig and rabbit: implications for arrhythmogenesis in human. *Circulation.* 104:951D956.
- Marban, E. 2002. Cardiac channelopathies. *Nature.*415:213D218.
- Nabauer, M., D. J. Beuckelmann, P. Uberfuhr, and G. Steinbeck. 1996. Regional differences in current density and rate-dependent properties of the transient outward current in subepicardial and subendocardial myocytes of human left ventricle. *Circulation.* 93:168D177.
- Paulussen, A., A. Raes, G. Matthijs, D. J. Snyders, N. Cohen, and J. Aerssens. 2002. A novel mutation (T65P) in the PAS domain of the human potassium channel HERG results in the long QT syndrome by trafficking deficiency. *J. Biol. Chem.*277:48610D48616.
- Priebe, L., and D. J. Beuckelmann. 1998. Simulation study of cellular electric properties in heart failure. *Circ. Res.*82:1206D1223.
- Sanguinetti, M. C., M. E. Curran, P. S. Spector, and M. T. Keating. 1996. Spectrum of HERG K-channel dysfunction in an inherited cardiac arrhythmia. *Proc. Natl. Acad. Sci. USA.*93:2208D2212.
- Sanguinetti, M. C., C. Jiang, M. E. Curran, and M. T. Keating. 1995. A mechanistic link between an inherited and an acquired cardiac arrhythmia: HERG encodes the potassium channel. *Cell.* 81:299D307.

- Sanguinetti, M. C., and N. K. Jurkiewicz. 1990. Two components of cardiac delayed rectifier K current. Differential sensitivity to block by class III antiarrhythmic agents. *Gen. Physiol.* 96:195-215.
- Seebohm, G., C. Lerche, A. E. Busch, and A. Bachmann. 2001. Dependence of  $f_{Ks}$  biophysical properties on the expression system. *Pflügers Arch.* 442:891-895.
- Sharp, A. A., M. B. O'Neil, L. F. Abbott, and E. Marder. 1993. Dynamic clamp: computer-generated conductances in real neurons. *Neurophysiol.* 69:992-995.
- Smith, P. L., T. Baukrowitz, and G. Yellen. 1996. The inward rectification mechanism of the HERG cardiac potassium channel. *Nature.* 379:833-836.
- Snyders, D. J., and A. Chaudhary. 1996. High affinity open channel block by dofetilide of HERG expressed in a human cell line. *Mol. Pharmacol.* 49:949-955.
- Sperelakis, N., and H. K. Shumaker. 1968. Phase-plane analysis of cardiac action potentials. *J. Electrocardiol.* 1:31-41.
- Tan, R. C., and R. W. Joyner. 1990. Electrotonic influences on action potentials from isolated ventricular cells. *Circ. Res.* 67:1071-1081.
- Ten Tusscher, K. H., D. Noble, P. J. Noble, and A. V. Panfilov. 2004. A model for human ventricular tissue. *Am. J. Physiol. Heart Circ. Physiol.* 286:H1573-H1589.
- Trudeau, M. C., J. W. Warmke, B. Ganetzky, and G. A. Robertson. 1995. HERG, a human inward rectifier in the voltage-gated potassium channel family. *Science* 269:92-95.
- Verkerk, A. O., M. W. Veldkamp, A. C. van Ginneken, and L. N. Bouman. 1996. Biphasic response of action potential duration to metabolic inhibition in rabbit and human ventricular myocytes: role of transient outward current and ATP-regulated potassium current. *Am. J. Physiol. Cell. Physiol.* 28:2443-2456.
- Wang, J., M. C. Trudeau, A. M. Zappia, and G. A. Robertson. 1998. Regulation of deactivation by an amino terminal domain in human ether-a-go-go-related gene potassium channels. *Gen. Physiol.* 12:637-647.
- Weerapura, M., S. Nattel, D. Chartier, R. Caballero, and T. E. Hebert. 2002. A comparison of currents carried by HERG, with and without coexpression of MiRP1, and the native rapid delayed rectifier current. Is MiRP1 the missing link? *Physiol.* 54:15-27.
- Wilders, R., R. Kumar, R. W. Joyner, H. J. Jongsma, E. E. Verheijck, D. Golod, A. C. van Ginneken, and W. N. Goolsby. 1996. Action potential conduction between a ventricular cell model and an isolated ventricular cell. *Biophys. J.* 70:281-295.
- Yamashita, T., Y. Murakawa, N. Hayami, E. Fukui, Y. Kasaoka, M. Inoue, and M. Omata. 2000. Short-term effects of rapid pacing on mRNA level of voltage-dependent K channels in rat atrium: electrical remodeling in paroxysmal atrial tachycardia. *Circulation.* 101:2007-2014.
- Zhou, Z., Q. Gong, B. Ye, Z. Fan, J. C. Makielski, G. A. Robertson, and C. T. January. 1998. Properties of HERG channels stably expressed in HEK 293 cells studied at physiological temperature. *Biophys. J.* 74:230-241.